



**HAL**  
open science

# Local structure and point defects-dependent Area-Selective Atomic Layer Deposition Approach for Facile Synthesis of p-Cu O/n-ZnO Segmented Nano-junctions

Claudia de Melo, Maud Jullien, Jaafar Ghanbaja, François Montaigne,  
Jean-François Pierson, Flavio Soldera, Federica Rigoni, Nils Almqvist, Alberto  
Vomiero, Frank Mücklich, et al.

► **To cite this version:**

Claudia de Melo, Maud Jullien, Jaafar Ghanbaja, François Montaigne, Jean-François Pierson, et al..  
Local structure and point defects-dependent Area-Selective Atomic Layer Deposition Approach for  
Facile Synthesis of p-Cu O/n-ZnO Segmented Nano-junctions. ACS Applied Materials & Interfaces,  
2018, 10 (43), pp.37671-37678. 10.1021/acsami.8b12584 . hal-03278609

**HAL Id: hal-03278609**

**<https://hal.science/hal-03278609>**

Submitted on 5 Jul 2021

**HAL** is a multi-disciplinary open access archive for the deposit and dissemination of scientific research documents, whether they are published or not. The documents may come from teaching and research institutions in France or abroad, or from public or private research centers.

L'archive ouverte pluridisciplinaire **HAL**, est destinée au dépôt et à la diffusion de documents scientifiques de niveau recherche, publiés ou non, émanant des établissements d'enseignement et de recherche français ou étrangers, des laboratoires publics ou privés.

# Local structure and point defects-dependent Area- Selective Atomic Layer Deposition Approach for Facile Synthesis of p-Cu<sub>2</sub>O/n-ZnO Segmented Nano-junctions

*Claudia de Melo<sup>†, ‡</sup>, Maud Jullien<sup>†</sup>, Jaafar Ghanbaja<sup>†</sup>, François Montaigne<sup>†</sup>, Jean-François Pierson<sup>†</sup>, Flavio Soldera<sup>‡</sup>, Federica Rigoni<sup>§</sup>, Nils Almqvist<sup>§</sup>, Alberto Vomiero<sup>§</sup>, Frank Mücklich<sup>‡</sup>,  
David Horwat<sup>†\*</sup>*

<sup>†</sup> Université de Lorraine, CNRS, IJL, F-54000 Nancy, France

<sup>‡</sup> Department of Materials Science and Engineering, Saarland University, D-66123 Saarbrücken,  
Germany

<sup>§</sup> Department of Engineering Sciences and Mathematics, Division of Materials Science, Luleå  
University of Technology, 971 87 Luleå, Sweden

KEYWORDS: area-selective deposition, atomic layer deposition, patterning, transmission electron microscopy, p-n junctions.

Area-selective atomic layer deposition (AS-ALD) has attracted much attention in recent years due to the possibility of achieving accurate patterns in nanoscale features which render this technique compatible with the continuous downscaling in nanoelectronic devices. The growth selectivity is achieved by starting from different materials and results (ideally) in localized growth of a single material. We propose here a new concept, more subtle and general, in which a property of the substrate is modulated to achieve localized growth of different materials. This concept is demonstrated by selective growth of high quality metallic Cu, and semiconducting Cu<sub>2</sub>O thin films achieved by changing the type of majority point defects in the ZnO underneath film exposed to the reactive species using a patterned bi-layer structure composed of highly conductive and highly resistive areas, as confirmed by transmission electron microscopy (TEM) and electron energy loss spectroscopy (EELS). The selective growth of these materials in a patterned ZnO/Al-doped ZnO substrate allows the fabrication of p-Cu<sub>2</sub>O/n-ZnO nano-junctions showing a non-linear rectifying behavior typical of a p-n junction, as confirmed by conductive atomic force microscopy (C-AFM). This process expands the spectra of materials that can be grown in a selective manner by ALD and opens up the possibility of fabricating different architectures taking advantage of the area-selective deposition. This offers variety of opportunities in the field of transparent electronics, catalysis and photovoltaics.

The continuous trend to miniaturization in microelectronics makes conventional patterning techniques challenging due to the extremely small features that are required. Conventional patterning is achieved by a top-down process consisting in the patterning of a resist film by lithography (photolithography, e-beam lithography, soft lithography, etc.) and a subsequent etching step. With technology approaching to the sub-10 nm scale, conventional patterning is

reaching its limit due to the difficulty in achieving a precise pattern, in particular when it comes to 2D and 3D nanostructures. Moreover, there are also some compatibility issues of certain materials with the developer or resist film and the etching step could be difficult when working with organic semiconductors and carbon-based materials.<sup>1</sup> These are the reasons why area selective deposition has gained a lot of attention. It limits the deposition of the material to the areas where it is desired, eliminating, or at least reducing, the number of lithography steps.

On the other hand, atomic layer deposition (ALD) has emerged as an important technique for depositing high quality thin films due to the self-limiting growth mechanism which enables an excellent surface coverage and conformal deposition on high aspect ratio structures. The fact that it depends strongly on the surface chemistry makes it a technique of choice for achieving area-selective deposition. Most of the approaches that have been used in the literature for achieving area-selective atomic layer deposition (AS-ALD) are based on the deactivation of part of the substrate by certain molecules or by self-assembly monolayers (SAMs), prior to ALD.<sup>2-7</sup> Successful deposition of ZnO and TiO<sub>2</sub> have been accomplished on Cu/Si patterned substrates by blocking the Cu surface using SAMs.<sup>5</sup> The selective growth of high-k gate dielectrics HfO<sub>2</sub> and ZrO<sub>2</sub> was demonstrated by Chen *et al.*<sup>7</sup> by using octadecyltrichlorosilane (ODTS). SiO<sub>2</sub> films were successfully grown on GeO<sub>2</sub> substrates with patterned Al<sub>2</sub>O<sub>3</sub>, using acetyl-acetate as growth inhibitor molecule<sup>3</sup> and Al<sub>2</sub>O<sub>3</sub> nanopatterns were selectively deposited on octadecylphosphonic acid (ODPA)-patterned Ti substrates.<sup>6</sup> AS-ALD of metallic films like Co,<sup>8</sup> Ni<sup>9</sup> and Pt<sup>10</sup> has been also successfully achieved by SAMs. Nevertheless, the use of SAMs is not without challenges. High deposition temperatures in thermal ALD affect the thermal stability of the SAMs, causing the loss of selectivity. Furthermore, SAMs are not compatible with plasma-assisted or ozone-based ALD,<sup>1</sup> which limits the number of material that can be deposited

in a selective manner by this method. In general, when referring to area-selective deposition it comes to deposition versus not deposition of a certain material on different surfaces or on the same surface but locally modified. However, for future nanoelectronics devices it is crucial to develop new approaches for simultaneous deposition of different materials in a selective manner on different surfaces in a straightforward way without adding new steps in the process. In this work we present the AS-ALD of Cu and Cu<sub>2</sub>O on ZnO and Al-doped ZnO films of controlled electronic conductivity. Our selective deposition approach is based on the inherent selectivity of the Cu(hfac)<sub>2</sub> precursor toward different ZnO surfaces. Therefore, no inhibitor or blocking molecules are needed. Hence, the process is simpler than any other patterning approaches and eliminates the problem of thermal stability related to SAMs. The modulation of the ZnO properties is achieved in this work by tuning the ZnO conductivity/type of majority point defects over a very large range (10<sup>-4</sup> to 10<sup>3</sup> S/cm) which, as we will demonstrate, determine the final material deposited: Cu or Cu<sub>2</sub>O. As already shown in the literature,<sup>11, 12</sup> the nature of the substrates can influence the growth and evolution of thin films. Moreover, the charge exchange at the interface between thermally-resistant inorganic substrates and film has shown its potential to strongly influence the phase formation in a selective way.<sup>13</sup> The area-selective deposition approach proposed here is very promising since the combination of metallic Cu films with semiconductor oxides (ZnO, Cu<sub>2</sub>O, or both) has many applications in different fields related with optoelectronics<sup>14</sup>, catalysis<sup>15</sup>, gas sensing<sup>16</sup> and photovoltaics.<sup>17</sup>

## **RESULTS AND DISCUSSION**

ZnO and Al-doped ZnO (AZO) films were deposited on (100) Si substrate by reactive magnetron sputtering of Zn and Zn<sub>98</sub>Al<sub>2</sub> targets, respectively, in different Ar-O<sub>2</sub> reactive mixtures. Figure 1a displays the conductivity of the films as a function of the position in the

chamber together with a schematic of the configuration used for deposition. Conductivity shows a minimum facing the magnetron axis (at 8 cm) and monotonously increases off-axis. The different O<sub>2</sub> partial pressures (PO<sub>2</sub>) used gave rise to different conductivities, lower for samples deposited at higher PO<sub>2</sub>. Moreover, doping ZnO with Al improves the conductivity of the films as it is evident from Figure 1a. Such change in conductivity is related to Al doping and modification of intrinsic point defect densities.<sup>18, 19, 20</sup>

Cu and Cu<sub>2</sub>O films were grown on top of the ZnO and AZO films by atomic layer deposition, using Cu(hfac)<sub>2</sub> as Cu precursor and water as reactant. Typical X-ray diffractograms of the samples obtained at a substrate temperature of 280 °C are shown in Figure 1b (the substrates used for the samples whose reported data appear in the figure are indicated by arrows in Figure 1a). Pure metallic Cu (green line), Cu<sub>2</sub>O (blue line) and a mixture of both phases (red line) were obtained depending on substrate conductivity. Some details about their structure, microstructure and synthesis conditions are given in the following before demonstrating their spatially-selected growth and discussing the mechanisms behind the formation of the different phases.

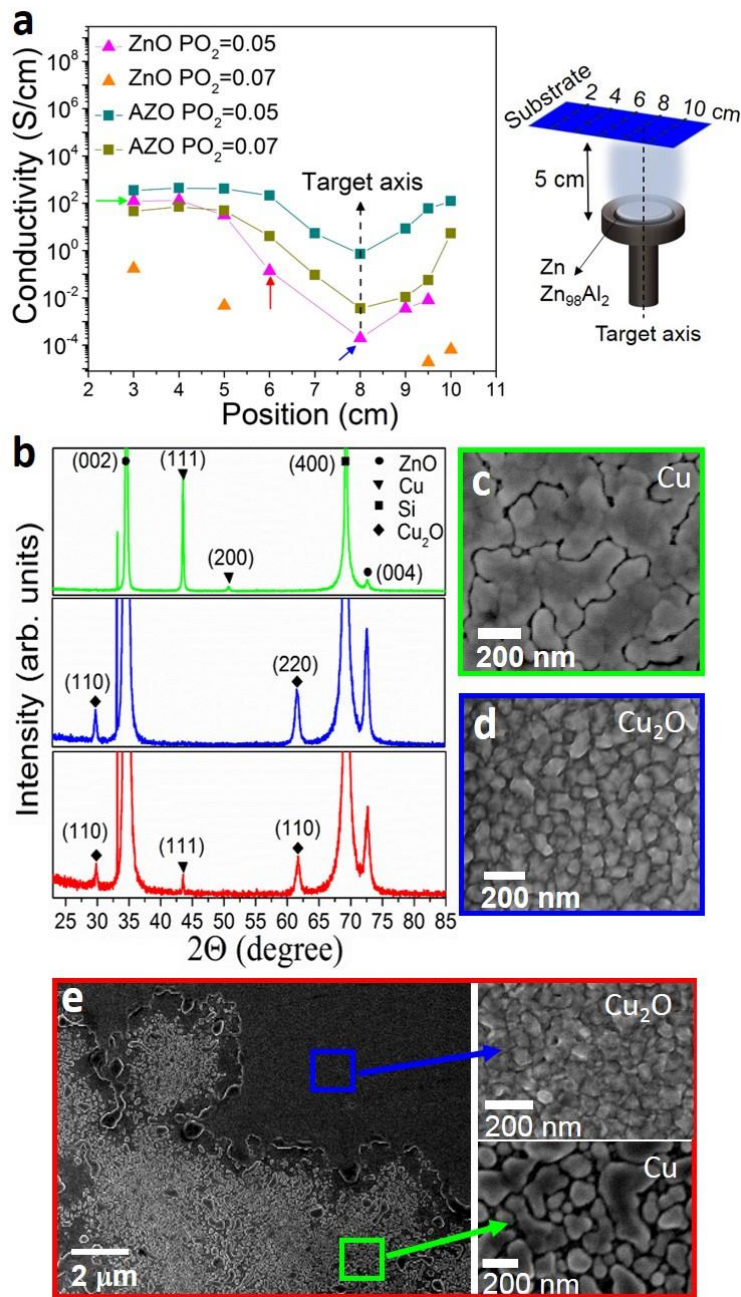


**Figure 1.** Conductivity of the ZnO and AZO films as a function of the position in the sputtering chamber and O<sub>2</sub> partial pressure (a), the schematic of the configuration used for the deposition is shown on the right. X-ray diffractograms of the samples after the ALD deposition at 280°C (b). Top-view SEM micrograph of the Cu film (c), the Cu<sub>2</sub>O film (d) and a film composed by a mixture of Cu and Cu<sub>2</sub>O (e). Remark: the conductivity of sample deposited using PO<sub>2</sub> = 0.07 Pa

was too high to be measured near the target axis, explaining why symbols were selected instead of connecting lines in Figure 1 (a) for this condition.

A top view SEM micrograph of a typical metallic Cu film (obtained after 10000 ALD cycles) is shown in Figure 1c. The film covers the entire substrate surface, except some discontinuities between crystallites, and consists in nanocrystalline Cu grains preferentially oriented in the [111] direction, as shown by the X-ray diffractogram of Figure 1b (green line). The length of coherent diffraction domains was determined from the integral breadth of the (111) diffraction peak, using Scherrer's equation. A value of 44 nm was obtained in good agreement with the film thickness of 48.9 nm, measured directly from the cross-section TEM micrograph of Figure 2a. A high resolution TEM (HRTEM) micrograph of this sample, with the corresponding fast Fourier transform pattern (FFT) is shown in Figure 2b. The interplanar spacing of the (111) planes was measured to be 0.211 nm, in good agreement with the value reported for cubic Cu (JCPDS 00-004-0836). For these samples a systematic study of the film morphology for different ALD cycles indicates a Volmer-Weber or island growth mode at early stages (see Figure S1 of supporting material).<sup>11</sup>

Figure 1d shows a top view SEM micrograph of a typical Cu<sub>2</sub>O film (10000 ALD cycles). In general, all the Cu<sub>2</sub>O samples deposited were textured with (110) planes parallel to the c-axis of ZnO, since only (110) and (220) peaks are observed in the X-ray diffractogram (Figure 1b, blue line). A thickness of around 40 nm was measured from the cross-section TEM micrograph shown in Figure 2c. A HRTEM micrograph of this sample is shown in Figure 2d, where the distance between (110) planes is measured to be 0.301 nm, in agreement with the values reported for cubic Cu<sub>2</sub>O (JCPDS 04-007-9767). The texture of this sample observed in the X-ray diffractogram suggests the possibility of an epitaxial relationship between Cu<sub>2</sub>O and ZnO. In

order to verify the later, HRTEM micrographs were taken at the interface between both layers (Figure 2e). The continuity of the lattice planes in the HRTEM micrograph and the corresponding fast Fourier transform patterns prove a local epitaxial relationship where  $[001] \text{Cu}_2\text{O} \parallel [010] \text{ZnO}$  films,  $(110) \text{Cu}_2\text{O} \parallel (001) \text{ZnO}$ . This orientation, although is not the typical of  $\text{Cu}_2\text{O}$  on  $\text{ZnO}$ , has already been observed in  $\text{Cu}_2\text{O}$  films grown by MOCVD using also  $\text{Cu}(\text{hfac})_2$  as Cu precursor.<sup>21</sup>

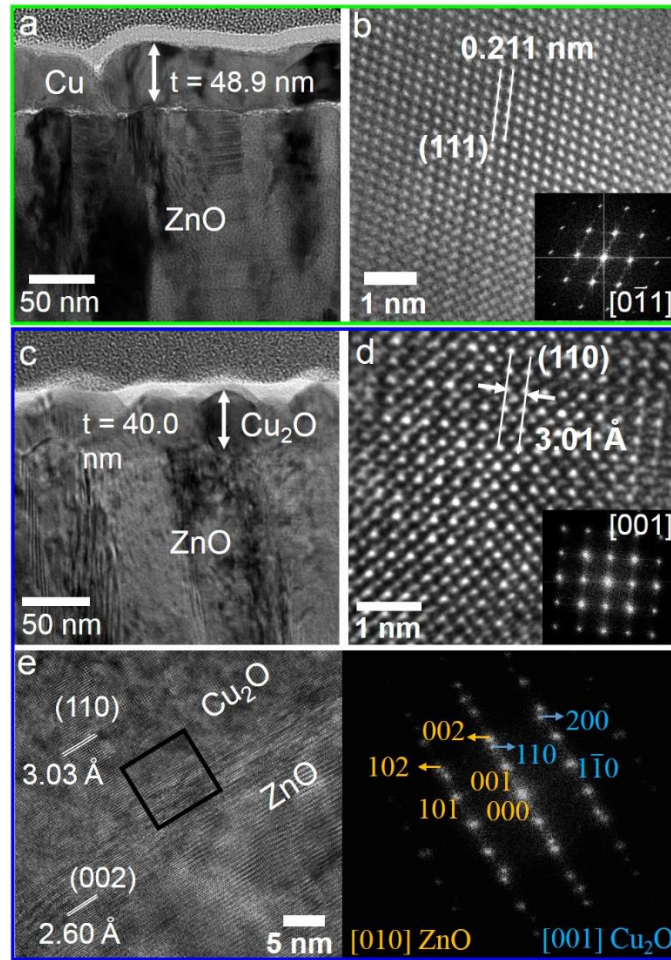


**Figure 2.** Cross-section TEM micrograph of the Cu (a) and the  $\text{Cu}_2\text{O}$  (c) films. HRTEM micrograph of the Cu (b) and the  $\text{Cu}_2\text{O}$  (d) films, the corresponding FFT patterns are shown at the inset. HRTEM micrograph of a  $\text{Cu}_2\text{O}$  sample (left) and the corresponding FFT patterns (right) at the  $\text{Cu}_2\text{O}/\text{ZnO}$  interface (region highlighted by a black square) (e).

Finally, the diffractogram of the sample composed of a mixture of  $\text{Cu}_2\text{O}$  and Cu is presented in Figure 1b (red line). The microstructure is confirmed by the presence of several peaks associated to (111) planes of Cu, and (110) and (220) planes of  $\text{Cu}_2\text{O}$ . Figure 1e is a top-view SEM micrograph of this samples. Two different morphologies are identified, one associated to metallic Cu and the other to  $\text{Cu}_2\text{O}$ , in agreement with obtained X-ray diffractograms.

It is worth mentioning that all these samples were grown simultaneously; hence, the deposition conditions were exactly the same for all of them, except the nature of the substrate used. Therefore, the phase change is driven by the nature of the substrates used. On highly conductive ZnO or AZO substrates ( $\sigma > 10 \text{ S/cm}$ ), Cu films are obtained, while  $\text{Cu}_2\text{O}$  is obtained on substrates with lower conductivity values ( $\sigma < 10^{-2} \text{ S/cm}$ ), and mixture of both phases for intermediate values. Additionally, on highly resistive ZnO substrates ( $\sigma \ll 10^{-4} \text{ S/cm}$ ), neither Cu nor  $\text{Cu}_2\text{O}$  deposition was observed. Therefore, it is possible to tune the deposited material or avoid deposition by simply changing the substrate conductivity.

The same study was repeated at 250 °C and 300 °C in order to analyze the influence of the growth temperature on the deposition process. Figure 3a summarizes all the results; the different phases obtained are plotted as a function of the ALD reaction chamber temperature and the substrate conductivity. No distinction was made between ZnO and AZO substrates, simply arranged in the figure depending on their electronic conductivity. For all temperatures studied Cu,  $\text{Cu}_2\text{O}$  and a mixture of Cu and  $\text{Cu}_2\text{O}$  could be obtained. However, the range of conductivity at which those phases appear is shifted depending on the substrate temperature. Higher temperatures favor the reduction of Cu into the precursor from  $\text{Cu}^{2+}$  to metallic  $\text{Cu}^0$ . This is the reason why at 300°C, the window for deposition of  $\text{Cu}_2\text{O}$  becomes smaller and metallic Cu is

obtained even for  $\sigma < 10^{-2}$  S/cm. In contrast, at low temperature, the reduction of  $\text{Cu}^{2+}$  into  $\text{Cu}^{1+}$  to form  $\text{Cu}_2\text{O}$  is extended to more conductive substrates.

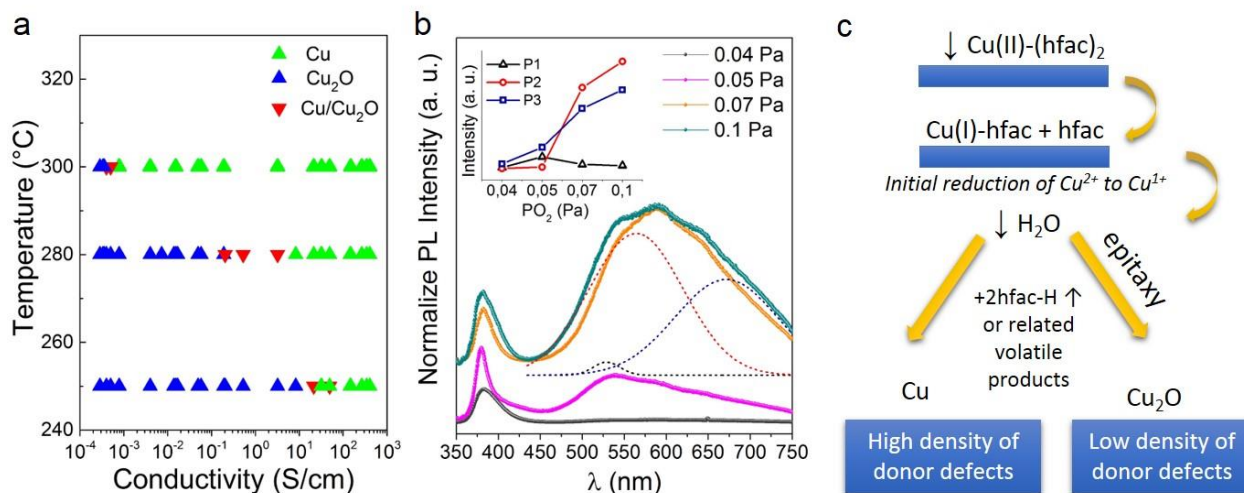


**Figure 3.** Diagram of the different phases deposited (Cu,  $\text{Cu}_2\text{O}$  or mixture) depending on the temperature and the substrate conductivity (a). Normalized photoluminescence spectra of ZnO films deposited at different  $\text{PO}_2$ , the evolution of the areal intensity of the defect bands with the oxygen partial pressure is presented at the inset (b). Schematic of the deposition mechanism for Cu and  $\text{Cu}_2\text{O}$  (c).

Several studies have reported the chemical vapor deposition of metallic Cu using  $\text{Cu}(\text{hfac})_2$  as Cu precursor. However, few reports concern atomic layer deposition of metallic Cu and even less  $\text{Cu}_2\text{O}$  deposition, using this precursor. In ALD, the precursors are pulsed separately and, therefore, the reactions taking place should be different from those in CVD, where precursors are injected simultaneously. The study of Cohen *et al.*<sup>11</sup> concerning the mechanism of copper chemical vapor deposition evidences that  $\text{Cu}(\text{hfac})_2$  dissociates on Ag substrates, as  $\text{Cu}(\text{I})\text{-hfac}$  and hfac. According to this study,  $\text{H}_2$  or alcohol are required to serve as proton source to allow the hfac ligands removal and Cu deposition. Lecohier *et al.*<sup>22</sup> also studied the mechanism of Cu deposition using  $\text{Cu}(\text{hfac})_2$  and water in presence of He or  $\text{H}_2$  carrier gases. Their results suggest

that H<sub>2</sub> is not indispensable as reducing agent since they were able to obtain clean metallic Cu films when He was used instead of H<sub>2</sub>. A different mechanism was proposed by Awaya et Arita<sup>23</sup> who suggested that Cu(hfac)<sub>2</sub> in presence of water, when adsorbed on the substrate, dissociates in Hhfac and CuO which is further reduced by H<sub>2</sub> to metallic Cu. Our results dismiss the idea of the formation of an intermediate oxide (CuO) further reduced into metallic Cu since we do not use any reducing agent after the water pulse and nevertheless metallic Cu films are obtained. Moreover, XPS measurement does not indicate the presence of Cu<sup>2+</sup>, neither in the case of metallic Cu nor for Cu<sub>2</sub>O films (see Figure S2 of supporting information).

The results presented above indicate undoubtedly a correlation between conductivity and area-selective deposition. Even if we have been speaking in terms of substrate conductivity, the possibility of achieving a temperature-selectivity process on non-conductive sapphire substrates (see Figure S3 of supporting information) suggests that this selectivity is correlated but probably not related directly to the level of conductivity. It is more likely related with local chemistry and/or structure that, in turn, influence the conductivity. Photoluminescence (PL) measurements were performed to the ZnO substrates obtained at different PO<sub>2</sub> (Figure 3b) to identify emitting defects present in the films. The peak at 380 nm is attributed to the near band edge emission of ZnO. The broad band that appears between 450 and 750 nm can be deconvoluted (from multiple-peak Gaussian fitting) into three bands: P1, P2 and P3, around 528 nm (green band), 564 nm (yellow band) and 660 nm (red band), respectively. P1 band has been ascribed to transitions between an Zn interstitial (Zn<sub>i</sub>) shallow level and oxygen vacancy (V<sub>O</sub>) level, P2 band is associated to oxygen interstitial (O<sub>i</sub>) and P3 band has been ascribed to transition from a shallow level to the O<sub>i</sub> level.

The evolution of the areal intensity of these three bands as a function of the  $\text{PO}_2$  is shown at the inset of Figure 3b. As can be seen, P1 decreases with the increasing of  $\text{PO}_2$  as a result of the decrease of  $V_{\text{O}}$  in more oxidative conditions. On the contrary, P2 and P3 bands increase with  $\text{PO}_2$  since generation of  $\text{O}_i$  defects occurs in more oxidative conditions. It is worth to note the remarkable difference between the signatures of ZnO sample deposited at  $\text{PO}_2$  of 0.05 and 0.07 Pa (the  $\text{PO}_2$  used for ZnO growth in this manuscript) resulting from the evolution of densities of the different point defects (higher density of  $\text{Zn}_i$  and  $V_{\text{O}}$  for deposition at 0.05 Pa and higher density of  $\text{O}_i$  defects for deposition at 0.07 Pa). In another study we could relate this evolution in the PL signal with  $\text{PO}_2$  to small, yet monotonous, changes in the oxygen content in the ZnO films.<sup>20</sup>  $V_{\text{O}}$  and  $\text{Zn}_i$  are considered as donor defects impacting the final n-type conductivity of the ZnO films. Furthermore, these donor defects can act as reducing agents for the  $\text{Cu}(\text{hfac})_2$  precursor inducing the selectivity of Cu vs.  $\text{Cu}_2\text{O}$ .  $V_{\text{O}}$  defects, for example, are known as active catalytic sites and electronically active centers<sup>24, 25</sup> that could play an important role in the  $\text{Cu}(\text{hfac})_2$  reduction.

We consider that the mechanism for  $\text{Cu}(\text{hfac})_2$  adsorption at the first ALD step is the same as proposed by Cohen *et al.* on Ag substrates:  $\text{Cu}(\text{hfac})_2$  is adsorbed as  $\text{Cu}(\text{I})\text{-hfac}$  intermediate and hfac. This first reduction of the precursor to  $\text{Cu}^{1+}$  is possibly due to the conductivity/density of donor defects of the ZnO substrate. When the conductivity of ZnO and density of donor defects are high enough,  $\text{Cu}^{1+}$  is further reduced into metallic Cu. In this step, water is fundamental as proton source to form a volatile compound and to remove the hfac ligands from the surface. On the contrary, when ZnO of low conductivity/low-density-of-donor-defects is used as substrate and water is pulsed into the chamber, Cu remains as  $\text{Cu}^{1+}$  to form  $\text{Cu}_2\text{O}$  (see the schematic of Figure 3c). In the case of  $\text{Cu}_2\text{O}$  formation, the epitaxial relation between film and substrate

seems to play also an important role in the film growth as will be demonstrated later. In the case of metallic substrates such as W and Zr films (see Figure S4 of supporting information) only metallic Cu could be obtained whatever the deposition temperature used. On silicon neither metallic Cu nor  $\text{Cu}_2\text{O}$  could be deposited (see Figure S5 of supporting information).

In order to take advantage of the selectivity of Cu and  $\text{Cu}_2\text{O}$  depending on the nature of the exposed surface, a bi-layer system was fabricated, patterned and functionalized. A low-conductive ZnO layer was deposited on top of a highly conductive AZO film with thickness of 145 nm and 323 nm, respectively, as is schematically represented in Figure 4a. Using e-beam lithography a pattern was formed by removing some regions of the ZnO top layer and, consequently, part of the AZO underneath layer was exposed, as depicted in Figure 4b. Then, the samples were introduced into the ALD chamber for selective deposition of Cu and  $\text{Cu}_2\text{O}$ . A temperature of 280 °C was used in order to obtain  $\text{Cu}_2\text{O}$  in the ZnO regions and metallic Cu in the exposed AZO regions (see Figure 4c, d).

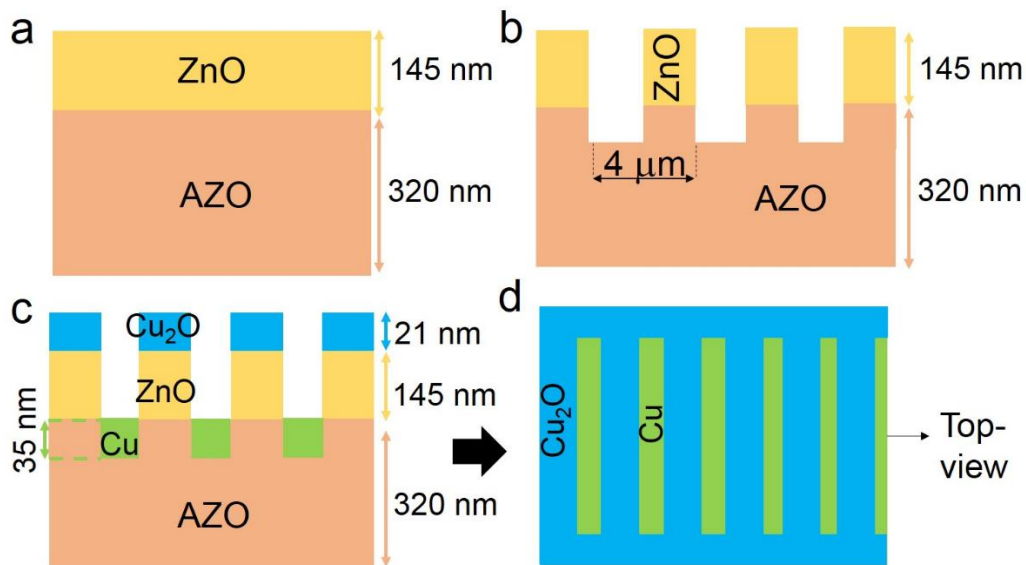


**Figure 4.** Schematic of the bi-layer structure (a) as-deposited, (b) after etching, and after ALD deposition in (c) cross-section and (d) top-view.

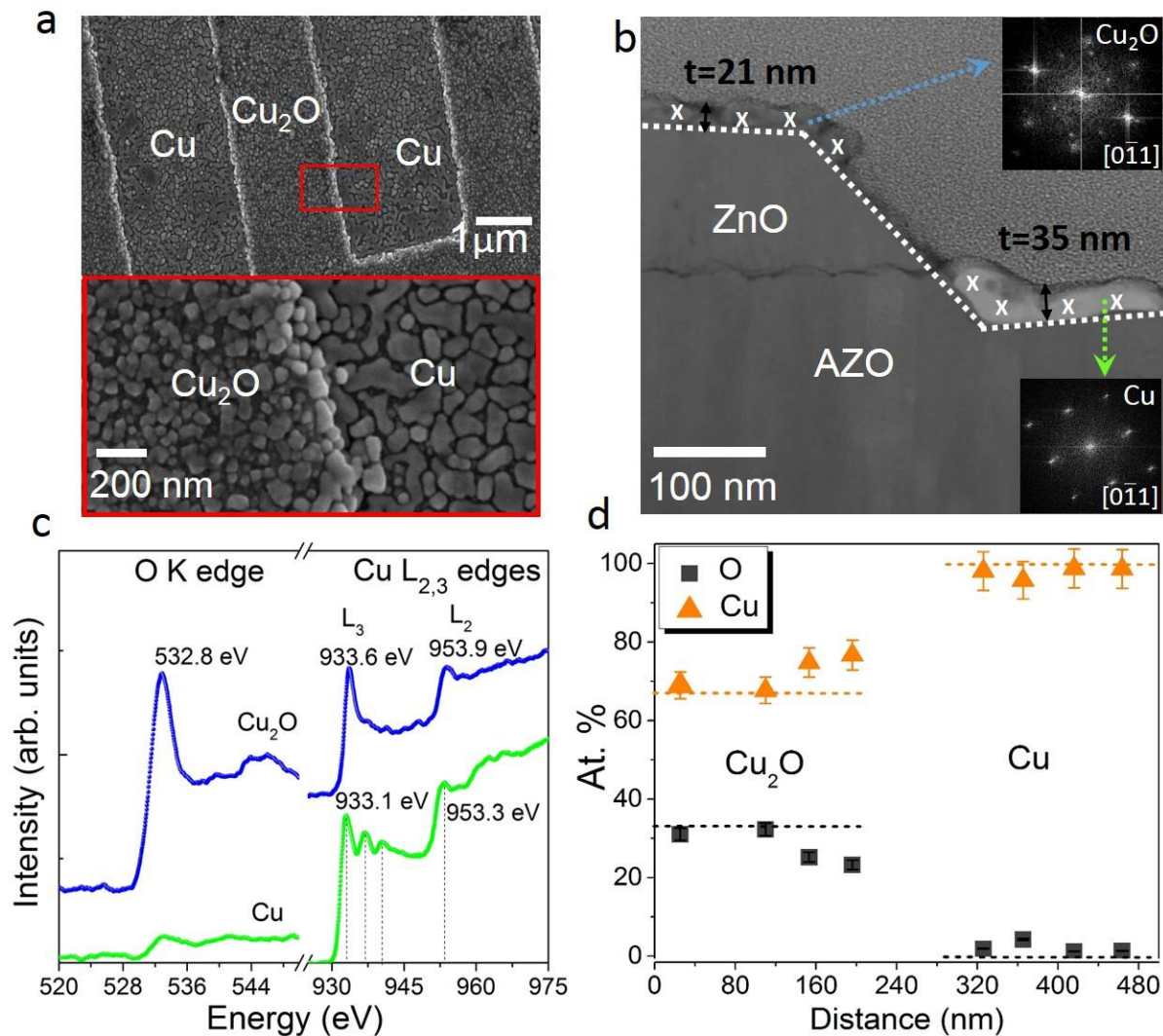


**Figure 5.** Top-view SEM micrograph of the bi-layer and magnified micrograph at the Cu<sub>2</sub>O/Cu interface highlighted by a red square (a). ADF-STEM micrograph of the bi-layer (b) with FFT patterns obtained from HRTEM micrographs in the Cu region (bottom inset) and the Cu<sub>2</sub>O region (top inset). EELS spectra at the O K and the Cu L<sub>2,3</sub> edges at the top (Cu<sub>2</sub>O) and bottom (Cu) of the bilayer (c). EDS composition profiles in the regions of the sample indicated by

crosses in b (dashed lines indicate the expected Cu and O concentrations for stoichiometric  $\text{Cu}_2\text{O}$  and for metallic Cu) (d).

In Figure 5a a top-view SEM micrograph taken to the sample after ALD deposition illustrates the different morphologies between the material deposited at the bottom of the wells (Cu) and the material deposited on top ( $\text{Cu}_2\text{O}$ ). In Figure 5b an annular dark field scanning transmission electron microscopy (ADF-STEM) micrograph at the well edge is displayed. The FFT patterns taken from HRTEM micrographs in  $\text{Cu}_2\text{O}$  (top inset) and Cu (bottom inset) regions, respectively, demonstrate the growth of metallic Cu on top of AZO and  $\text{Cu}_2\text{O}$  on top of ZnO.

Electron energy loss spectroscopy (EELS) in transmission mode was performed in both regions. The energy loss near edge structure (ELNES) spectra at O K and Cu  $L_{2,3}$  edges are shown in Figure 5c. The spectra obtained at Cu  $L_{2,3}$  edges in Cu and  $\text{Cu}_2\text{O}$ , are in good agreement with those reported in the literature.<sup>26,27,28</sup> The  $\text{Cu}_2\text{O}$  ELNES spectrum is characterized by the  $L_{2,3}$  white lines at 953.9 eV and 933.6 eV, respectively. At the Cu region the spectrum is formed by the  $L_3$  line around 933.1 eV, followed by two less intense peaks around 937.1 and 940.4 eV, which have been identified in the literature as the 4p-4d hybridization structure.<sup>29</sup> The  $L_2$  line appears at 953.3 eV, followed by a wide band that rises around 962.6 eV and which has been ascribed to a 4f band with some d character.<sup>29</sup> The features of the spectra and the peak position at the O K edge confirm that pure  $\text{Cu}_2\text{O}$  was deposited on top of ZnO.<sup>30</sup> In the case of Cu, a very small, poorly defined edge is observed that we ascribe to the presence of some oxidized Cu in the form of CuO at the surface of the Cu film.

Composition profiles at the surface obtained by EDS analysis in STEM mode at the same region where the STEM micrograph was taken further confirm the deposition of  $\text{Cu}_2\text{O}$  on the ZnO layer and Cu in the AZO film (see Figure 5d). The film deposited on top of ZnO contains

32 at. % O and 68 at. % Cu, very close to the stoichiometry of Cu<sub>2</sub>O, even if slightly different values of 28 at. % O and 72 at. % Cu, are obtained close to the well edge. On the other hand, on top of AZO values around 99% for the Cu and 1% for the O were obtained, confirming the deposition of metallic Cu in this region. The detection of some oxygen even in minor quantity could be related to the presence of some CuO formed at the surface of the Cu film.

It is worth mentioning that the Cu layer stops exactly at the interface with the low-conductive ZnO film, as can be seen in Figure 5b. In the case of the Cu<sub>2</sub>O, deposition is somehow inhibited in the lateral walls of the ZnO films, there is deposition on the corner, but then there is not more Cu<sub>2</sub>O along the rest of the lateral wall. This result indicates that the local epitaxial relationship between Cu<sub>2</sub>O films on ZnO substrates plays an important role in Cu<sub>2</sub>O formation. Indeed, Cu<sub>2</sub>O more easily grows epitaxially on (001) ZnO with [001] Cu<sub>2</sub>O || [010] ZnO films, (110) Cu<sub>2</sub>O || (001) ZnO (as was shown in Figure 2e) and this is the reason why Cu<sub>2</sub>O deposition is blocked at the edge of the ZnO plateau, in contrast with the deposition of metallic Cu that extends up to the AZO/ZnO interface regardless of the orientation relationship. This is in line with the possibility to deposit Cu<sub>2</sub>O on c-axis sapphire (see Figure S2 in the supplementary information).

Using this selective area deposition process, we have tested and achieved selective growth of Cu and Cu<sub>2</sub>O features of lateral sizes from ca. 200 nm up to several centimeters. Figure S6 of supporting information highlights this for two different lateral sizes.

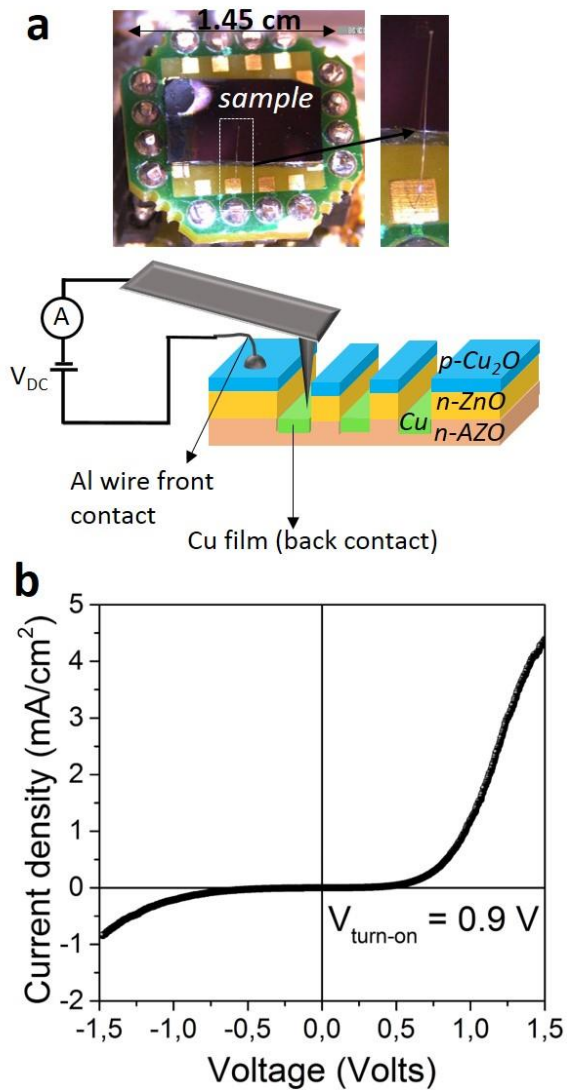


**Figure 6.** Schema of the sample configuration for the C-AFM measurements and the electrical contacts (a). Current density - voltage characteristics of the device on dark at room temperature (b).

This architecture achieved by this relatively simple method is interesting for the fabrication of segmented  $Cu_2O/ZnO/AZO$  nano-junctions. The Cu film deposited on top of the AZO layer works as electrical contact. The suppression of  $Cu_2O$  deposition observed on the ZnO side walls eliminates the risk of short circuit between  $Cu_2O$  on ZnO and Cu on AZO. Due to the extremely

small features in this sample, traditional photovoltaics measurements are not suitable. Therefore, in order to test the rectifying behavior of these nano-junctions, C-AFM was performed. The small chip of Figure 6a was used as substrate-holder. An Al wire was attached on top of the  $\text{Cu}_2\text{O}$  region and weld to the exterior contact of this chip to work as front contact (see amplified picture in Figure 6a). Then, the AFM tip was put in contact with the Cu film, working as back contact (see schema in Figure 6a). Figure 6b shows the current density - voltage (JV) curve measured on dark at room temperature by C-AFM. A non-linear rectifying behavior characteristic of a p-n junction formed between  $\text{Cu}_2\text{O}$  and ZnO is observed. A turn-on voltage of approximately 0.9 V is obtained. Therefore, the method we have reported enables easy fabrication of segmented p- $\text{Cu}_2\text{O}$ /n-ZnO nano-junctions with simultaneous deposition of the p- $\text{Cu}_2\text{O}$  layer and of the metallic Cu contact using AS-ALD on a patterned AZO/ZnO bilayer. It opens up new possibilities for the nanofabrication of semiconductor devices.

## CONCLUSIONS

The presented results offer a novel approach for the AS-ALD where the properties of the substrate are modulated (in this case by tuning the substrate conductivity/density of donor defects) in order to achieve the local deposition of different materials in different regions. As a proof of concept, a bi-layer structure made of a low-conductive ZnO layer on top of a highly-conductive AZO film, was fabricated, patterned and functionalized. HRTEM, EELS and EDS confirm that area-selective deposition of metallic Cu on highly conductive areas and  $\text{Cu}_2\text{O}$  on low-conductive areas was achieved. In this approach, deposition of different materials is obtained, but “traditional” selectivity is kept by simply using highly resistive ZnO films as substrate to avoid local growth.

This selective deposition on patterned ZnO/AZO substrates allow the successful fabrication of Cu<sub>2</sub>O/ZnO/AZO nano-junctions. These results are very promising for low-cost all-oxide transparent microelectronics. Furthermore, the deposition of several Cu<sub>2</sub>O/ZnO nano-junctions by this method on a transparent substrate would produce a segmented photovoltaic architecture, promising for building-integrated photovoltaics.

This configuration is a first approach of the many different ones than could be achieved. Defining otherwise the conductivity zones one would create different interfaces, allowing the formation of different architectures. All in all, this method provides an understanding of how AS-ALD can be further improved and extended to a wider range of materials. Because reduction /oxidation of the precursors are general processes involved in the deposition of thin films by ALD, we expect that the method proposed here can be extended to selectively deposit other metals and compounds than Cu and Cu<sub>2</sub>O.

## **EXPERIMENTAL SECTION**

*Synthesis of ZnO and AZO films.* ZnO and AZO film were deposited on (100) Si substrates by DC reactive magnetron sputtering of Zn (99.995% of purity) and Zn<sub>98</sub>Al<sub>2</sub> (99.995 % of purity for Zn and 99.999 % for Al) targets respectively in different Ar-O<sub>2</sub> reactive mixtures. The silicon substrates were placed along the radial direction of a rotating substrate holder parallel to the target surface as shown in Figure 1. The reaction chamber was pumped down through a turbo-molecular pump allowing a base pressure of 10<sup>-3</sup> Pa. The Ar flow rate was kept constant at 50 sccm and different O<sub>2</sub> partial pressures of 0.05 and 0.07 Pa were used. The total pressure was close to 0.5 Pa. Both targets were powered by an Advanced Energy MDX 1.5 kW DC generator and the discharge current applied was of 0.07 A.

*Copper and copper oxide deposition.* Cu and Cu<sub>2</sub>O films were deposited on ZnO and AZO films in a ALD PICOSUN™ R-200 Advanced reactor using copper (II) hexafluoro-acetylacetonate, Cu(hfac)<sub>2</sub> (99.99+%-Cu, Stream Chemicals) as Cu precursor and water vapor as reactant. The Cu(hfac)<sub>2</sub> was sublimated at 70°C and the water was kept at 18°C. The reaction chamber pressure was 10 hPa and the temperature was varied from 250°C up to 300°C. N<sub>2</sub> was used as carrier and purge gas with a flow rate of 120 sccm in the Cu(hfac)<sub>2</sub> line and 150 sccm in the H<sub>2</sub>O line. The boosting mode was used in order to enhance the vapor pressure of the Cu(hfac)<sub>2</sub> precursor. The optimized deposition sequence consists of 3 s of Cu(hfac)<sub>2</sub> / 6 s of N<sub>2</sub> purge/ 3 s of H<sub>2</sub>O / 6 s of N<sub>2</sub> purge, and the number of cycles was varied between 1500 and 10000. Metallic Cu or Cu<sub>2</sub>O were obtained depending on both, the temperature and the conductivity of the substrate.

*Lithography.* For the patterning of the bi-layer structure we use the e-beam lithography and ion beam etching. First a polymethyl methacrylate (PMMA)5% (ARP672.05) was coated at the surface of the bi-layer and was heated at 180°C by 5 min. Then, the surface was exposed to the electron beam using 20 kV with doses ranging from 80-160 μC/cm<sup>2</sup>. This step was follow by an immersion of the film into a liquid developer formed by a mixture of Methyl Isobutyl Kethone (MIBK) and isopropyl alcohol (IPA) for 60 s and then the sample was rinsed in IPA solution for 30 s. This process allows to remove the part of the mask exposed to the e-beam. Then, ion beam etching (200 eV Ar ions) was used to etch the unmasked areas down to the AZO layer. Finally, O<sub>2</sub> plasma was used to remove any resist from the surface.

*Characterization techniques.* X - rays diffractograms in the Bragg-Brentano configuration were taken using a Bruker D8 Advanced diffractometer with Cu K<sub>α1</sub> radiation (λ=1.5406 Å). Conductivity measurements were performed in a four-point probe system. To analyze the

microstructure of the samples scanning electron micrographs were taken in a Philips XL-30 S-FEG SEM at 5 kV. Transmission electron microscopy (TEM) was performed by a JEOL ARM 200-Cold FEG (point resolution 0.19 nm). For this analysis, cross-section TEM samples of films were prepared using a focused ion beam (FIB)-scanning electron microscope (SEM) dual beam system (FEI Helios 600). The samples were obtained with the lift-out technique. Preparation and thinning of the foil were done with an acceleration voltage of 30 kV. However, last step of the thinning was done with acceleration voltage of 5kV, in order to minimize any possible artifact like amorphization or ion implantation. Composition profiles were obtained by EDS in the TEM. EELS experiments were performed in diffraction mode. The spectrometer was set to an energy dispersion of 0.05 eV/channel. The condenser aperture, spectrometer entrance and camera length were 150  $\mu\text{m}$ , 2.5 mm and 4 cm, respectively leading to a collection half angle of 20 mrad and an energy resolution of 0.5 eV, measured at full width at half maximum (FWHM) of the zero loss peak. X-ray photoelectron spectroscopy was performed to the samples using Mg  $K\alpha$  radiation at 1.25 keV, after 2 min of Ar-etching at 5 keV to remove the contamination at the surface. The C-AFM measurements were performed at ambient conditions with a NTEGRA AFM (NT-MDT) in contact mode using a N-doped diamond coated probe (DCP20 series) with a tip height of 10  $\mu\text{m}$ , nominal tip radius of 100 nm and nominal spring constant of 48 N/m. The presence of defects was investigated by photoluminescence analyses in the UV and visible ranges with laser excitation at 325 nm.

ASSOCIATED CONTENT

**Supporting Information.** Additional characterization data and figures (SEM micrographs, X-ray photoelectron spectroscopy, and examples of Cu<sub>2</sub>O and Cu deposition in other substrates) (PDF).

## AUTHOR INFORMATION

### Corresponding Author

\*E-mail: [david.horwat@univ-lorraine.fr](mailto:david.horwat@univ-lorraine.fr)

### ORCID

David Horwat: 0000-0001-7938-7647

### Author Contributions

The manuscript was written through contributions of all authors. All authors have given approval to the final version of the manuscript. DH, MJ, FMu, FMo, JFP planned and supervised the study. FS performed the FIB preparation, JG the HR-TEM and EELS analyses and FMo performed the e-beam lithography and ion beam etching. FR, NA and AV performed the C-AFM measurements and analysis. CDM conducted the experiments and wrote the manuscript. All authors discussed the results and revised the manuscript.

### Funding Sources

Erasmus Mundus Ph.D. fellowship doctoral program DocMASE (Project 2015-03)

*Université franco-allemande* (UFA) PhD track "German/French Graduate School in Materials Science and Engineering" (PhD02-14)

Carl Tryggers Foundation (CTS16:13, CTS17:24)

Kempe Foundations (SMK-2546)

Knut and Alice Wallenberg Foundation

Notes

The authors declare no competing financial interest.

## ACKNOWLEDGMENT

The Davm competence center of IJL is deeply acknowledged for access to ALD deposition facility. C. de Melo would like to thank the European Commission for “Erasmus Mundus” Ph.D. fellowship with the DocMASE project and to the Université franco-allemande (UFA) PhD track "German/French Graduate School in Materials Science and Engineering" for the mobility aids. The authors want to thanks Alexandre Boucher (University of Lorraine) for help with the XPS measurements, Sylvie Migot (University of Lorraine) for her help with the preparation of TEM lamella using FIB, Laurent Badie (University of Lorraine) for his help with the deposition of Al contact, Patrice Miska and W. Chamorro (University of Lorraine) are acknowledged for their help with PL measurements. F. Rigoni acknowledges the Carl Tryggers Foundation (CTS16:13, CTS17:24) for a postdoctoral fellowship. A. Vomiero and N. Almqvist acknowledge the Kempe Foundations for funding the AFM equipment (SMK-2546). A. Vomiero and N. Almqvist acknowledge the Knut and Alice Wallenberg Foundation for partial funding.

## ABBREVIATIONS

AS-ALD, area-selective atomic layer deposition; ALD, atomic layer deposition; TEM, transmission electron microscopy; EELS, electron energy loss spectroscopy; SAMs, self-assembly monolayers; AZO, Al-doped ZnO;  $PO_2$ ,  $O_2$  partial pressures; HRTEM, high resolution transmission electron microscopy; FFT, fast Fourier transform pattern; PL, photoluminescence;

ADF-STEM, annular dark field scanning transmission electron microscopy; ELNES, energy loss near edge structure; C-AFM, conductive atomic force microscopy.

## REFERENCES

- (1) Mackus, A. J. M.; Bol, A. A.; Kessels, W. M. M. The Use of Atomic Layer Deposition in Advanced Nanopatterning. *Nanoscale* **2014**, *6* (19), 10941–10960.
- (2) Chen, R.; Kim, H.; McIntyre, P. C.; Porter, D. W.; Bent, S. F. Achieving Area-Selective Atomic Layer Deposition on Patterned Substrates by Selective Surface Modification. *Appl. Phys. Lett.* **2005**, *86* (19), 191910.
- (3) Marnett, A.; Merckx, M. J. M.; Karasulu, B.; Roozeboom, F.; Kessels, W. (Erwin) M. M.; Mackus, A. J. M. Area-Selective Atomic Layer Deposition of SiO<sub>2</sub> Using Acetylacetonone as a Chemoselective Inhibitor in an ABC-Type Cycle. *ACS Nano* **2017**, *11* (9), 9303–9311.
- (4) Park, M. H.; Jang, Y. J.; Sung-Suh, H. M.; Sung, M. M. Selective Atomic Layer Deposition of Titanium Oxide on Patterned Self-Assembled Monolayers Formed by Microcontact Printing. *Langmuir* **2004**, *20* (6), 2257–2260.
- (5) Minaye Hashemi, F. S.; Birchansky, B. R.; Bent, S. F. Selective Deposition of Dielectrics: Limits and Advantages of Alkanethiol Blocking Agents on Metal–Dielectric Patterns. *ACS Appl. Mater. Interfaces* **2016**, *8* (48), 33264–33272.
- (6) Seo, S.; Yeo, B. C.; Han, S. S.; Yoon, C. M.; Yang, J. Y.; Yoon, J.; Yoo, C.; Kim, H.; Lee, Y.; Lee, S. J.; Myoung, J.; Lee, H.; Kim, W.; Oh, I.; Kim, H. Reaction Mechanism of Area-Selective Atomic Layer Deposition for Al<sub>2</sub>O<sub>3</sub> Nanopatterns. *ACS Appl. Mater. Interfaces* **2017**, *9* (47), 41607–41617.

- (7) Chen, R.; Kim, H.; McIntyre, P. C.; Bent, S. F. Self-Assembled Monolayer Resist for Atomic Layer Deposition of HfO<sub>2</sub> and ZrO<sub>2</sub> High-κ Gate Dielectrics. *Appl. Phys. Lett.* **2004**, *84* (20), 4017–4019.
- (8) Lee, H.-B.-R.; Kim, W.-H.; Lee, J. W.; Kim, J.-M.; Heo, K.; Hwang, I. C.; Park, Y.; Hong, S.; Kim, H. High Quality Area-Selective Atomic Layer Deposition Co Using Ammonia Gas as a Reactant. *J. Electrochem. Soc.* **2010**, *157* (1), D10–D15.
- (9) Kim, W.-H.; Lee, H.-B.-R.; Heo, K.; Lee, Y. K.; Chung, T.-M.; Kim, C. G.; Hong, S.; Heo, J.; Kim, H. Atomic Layer Deposition of Ni Thin Films and Application to Area-Selective Deposition. *J. Electrochem. Soc.* **2011**, *158* (1), D1–D5.
- (10) Hong, J.; Porter, D. W.; Sreenivasan, R.; McIntyre, P. C.; Bent, S. F. ALD Resist Formed by Vapor-Deposited Self-Assembled Monolayers. *Langmuir* **2007**, *23* (3), 1160–1165.
- (11) Cohen, S. L.; Liehr, M.; Kasi, S. Mechanisms of Copper Chemical Vapor Deposition. *Appl. Phys. Lett.* **1992**, *60* (1), 50–52.
- (12) Lemaire, P. C.; King, M.; Parsons, G. N. Understanding Inherent Substrate Selectivity during Atomic Layer Deposition: Effect of Surface Preparation, Hydroxyl Density, and Metal Oxide Composition on Nucleation Mechanisms during Tungsten ALD. *J. Chem. Phys.* **2016**, *146* (5), 052811.
- (13) Horwat, D.; Dehmas, M.; Gutiérrez, A.; Pierson, J.-F.; Anders, A.; Soldera, F.; Endrino, J.-L. Efficient, Low Cost Synthesis of Sodium Platinum Bronze Na<sub>x</sub>Pt<sub>3</sub>O<sub>4</sub>. *Chem. Mater.* **2012**, *24* (13), 2429–2432.
- (14) Sivaramakrishnan, K.; Theodore, N. D.; Moulder, J. F.; Alford, T. L. The Role of Copper in ZnO/Cu/ZnO Thin Films for Flexible Electronics. *J. Appl. Phys.* **2009**, *106* (6), 063510.

- (15) Behrens, M.; Studt, F.; Kasatkin, I.; Köhl, S.; Hävecker, M.; Abild-Pedersen, F.; Zander, S.; Girgsdies, F.; Kurr, P.; Knief, B.-L.; Tovar, M.; Fischer, R. W.; Nørskov, J. K.; Schlögl, R. The Active Site of Methanol Synthesis over Cu/ZnO/Al<sub>2</sub>O<sub>3</sub> Industrial Catalysts. *Science* **2012**, *336* (6083), 893–897.
- (16) Lunkenbein, T.; Schumann, J.; Behrens, M.; Schlögl, R.; Willinger, M. G. Formation of a ZnO Overlayer in Industrial Cu/ZnO/Al<sub>2</sub>O<sub>3</sub> Catalysts Induced by Strong Metal–Support Interactions. *Angew. Chem.* **2015**, *127* (15), 4627–4631.
- (17) Jeong, S. S.; Mittiga, A.; Salza, E.; Masci, A.; Passerini, S. Electrodeposited ZnO/Cu<sub>2</sub>O Heterojunction Solar Cells. *Electrochimica Acta* **2008**, *53* (5), 2226–2231.
- (18) Jullien, M.; Horwat, D.; Manzeh, F.; Escobar Galindo, R.; Bauer, P.; Pierson, J. F.; Endrino, J. L. Influence of the Nanoscale Structural Features on the Properties and Electronic Structure of Al-Doped ZnO Thin Films: An X-Ray Absorption Study. *Sol. Energy Mater. Sol. Cells* **2011**, *95* (8), 2341–2346.
- (19) Horwat, D.; Billard, A. Effects of Substrate Position and Oxygen Gas Flow Rate on the Properties of ZnO: Al Films Prepared by Reactive Co-Sputtering. *Thin Solid Films* **2007**, *515* (13), 5444–5448.
- (20) Chamorro, W.; Horwat, D.; Pigeat, P.; Miska, P.; Migot, S.; Soldera, F.; Boulet, P.; Mücklich, F. Near-Room Temperature Single-Domain Epitaxy of Reactively Sputtered ZnO Films. *J. Phys. Appl. Phys.* **2013**, *46* (23), 235107.
- (21) Jeong, S.; Aydil, E. S. Heteroepitaxial Growth of Cu<sub>2</sub>O Thin Film on ZnO by Metal Organic Chemical Vapor Deposition. *J. Cryst. Growth* **2009**, *311* (17), 4188–4192.

- (22) Lecohier, B.; Calpini, B.; Philippoz, J. -M.; Stumm, T.; van den Bergh, H. Selective Low Pressure Chemical Vapor Deposition of Copper: Effect of Added Water Vapor in Hydrogen or Helium Carrier Gas. *Appl. Phys. Lett.* **1992**, *60* (25), 3114–3116.
- (23) Awaya, N.; Arita, Y. Accelerated-Deposition Rate and High-Quality Film Copper Chemical Vapor Deposition Using a Water Vapor Addition to a Hydrogen and Cu(HFA)<sub>2</sub> Reaction System. *Jpn. J. Appl. Phys.* **1993**, *32* (9R), 3915–3919.
- (24) Brillson, L. J.; Mosbacker, H. L.; Douth, D. L.; Dong, Y.; Fang, Z.-Q.; Look, D. C.; Cantwell, G.; Zhang, J.; Song, J. J. Nanoscale Depth-Resolved Cathodoluminescence Spectroscopy of ZnO Surfaces and Metal Interfaces. *Superlattices Microstruct.* **2009**, *45* (4), 206–213.
- (25) French, S. A.; Sokol, A. A.; Bromley, S. T.; Catlow, C. R. A.; Sherwood, P. Identification and Characterization of Active Sites and Their Catalytic Processes—the Cu/ZnO Methanol Catalyst. *Top. Catal.* **2003**, *24* (1–4), 161–172.
- (26) Henzler, K.; Heilemann, A.; Kneer, J.; Guttman, P.; Jia, H.; Bartsch, E.; Lu, Y.; Palzer, S. Investigation of Reactions between Trace Gases and Functional CuO Nanospheres and Octahedrons Using NEXAFS-TXM Imaging. *Sci. Rep.* **2015**, *5*, 17729.
- (27) Chamorro, W.; Shyju, T. S.; Boulet, P.; Migot, S.; Ghanbaja, J.; Miska, P.; Kuppusami, P.; Pierson, J. F. Role of Cu<sup>+</sup> on ZnS:Cu p-Type Semiconductor Films Grown by Sputtering: Influence of Substitutional Cu in the Structural, Optical and Electronic Properties. *RSC Adv.* **2016**, *6* (49), 43480–43488.
- (28) Wang, Y.; Lany, S.; Ghanbaja, J.; Fagot-Revurat, Y.; Chen, Y. P.; Soldera, F.; Horwat, D.; Mücklich, F.; Pierson, J. F. Electronic Structures of Cu<sub>2</sub>O, Cu<sub>4</sub>O<sub>3</sub>, and CuO: A Joint Experimental and Theoretical Study. *Phys. Rev. B* **2016**, *94* (24), 245418.

- (29) Leapman, R. D.; Grunes, L. A.; Fejes, P. L. Study of the  $L_{23}$  Edges in the 3d Transition Metals and Their Oxides by Electron-Energy-Loss Spectroscopy with Comparisons to Theory. *Phys. Rev. B* **1982**, *26* (2), 614–635.
- (30) Gurevich, A. B.; Bent, B. E.; Teplyakov, A. V.; Chen, J. G. A NEXAFS Investigation of the Formation and Decomposition of CuO and Cu<sub>2</sub>O Thin Films on Cu (100). *Surf. Sci.* **1999**, *442* (1), L971–L976.